Theory and numerical simulation of *n*th-order cascaded Raman fiber lasers

Stuart D. Jackson

Optical Fibre Technology Centre, Australian Photonics Cooperative Research Centre, The University of Sydney, 206 National Innovation Centre, Australian Technology Park, Eveleigh, 1430 Sydney, Australia

Paul H. Muir

Department of Mathematics and Computing Science, Saint Mary's University, Halifax, Nova Scotia, Canada B3H 3C3

Received November 27, 2000; revised manuscript received March 16, 2001

Using the classical treatment of the stimulated Raman-scattering process, we use a theoretical model to simulate the operation of an *n*th-order cascaded Raman fiber laser. We introduce the partial differential equations employed to describe the propagation and time dependence of the forward and reverse-propagating fields of an *n*th-order cascaded Raman fiber laser. Under steady-state conditions, these equations form the well-known system of first-order, nonlinear boundary-value ordinary differential equations, with separated boundary conditions. We solve this system of equations numerically with the use of mono-implicit Runge–Kutta methods within a defect-control framework. We consider cascaded Raman fiber lasers of orders 2 through 5 and examine the parameters that influence the operation of these devices. We also provide preliminary results on the investigation of a time-dependent model in which the pump power is assumed to vary periodically with time. The associated system of first-order, hyperbolic, partial differential equations is treated by employing a transverse method-of-lines algorithm; the time derivatives are discretized with a finite-difference scheme, yielding a large system of boundary-value ordinary differential equations. We establish that for sinusoidal modulation of the pump the Stokes cavity modes exhibit antiphase dynamics typical of a system of locally coupled nonlinear oscillators.

OCIS codes: 140.3510, 140.3430, 140.3550, 190.4370.

1. INTRODUCTION

Since the first classical description of a cw Raman fiber laser,[1] considerable progress has also been made experimentally with a number of successful demonstrations already producing high power and relatively high efficiency.[2–10] With these devices, high-power cw pump light from a double-clad fiber laser is launched into a long low-loss silica-based fiber that can be doped with either GeO_2 or P_2O_5 to exploit a potentially higher Raman gain or a wider frequency shift from the pump frequency, respectively. With the application of Bragg gratings designed to resonate the Stokes light, efficient downshifted single-transverse-mode laser radiation is produced. Cascaded Raman fiber lasers are therefore highly suitable for a number of direct and indirect applications such as the pumping of Raman fiber amplifiers and other fiber lasers.

Cw cascaded Raman fiber lasers are generally described by a first-order system of nonlinear two-point boundary-value ordinary differential equations (BVODEs) with the boundary conditions relating to the reflection coefficients of the mirrors at each end of the fiber laser. Past theoretical investigations of these lasers[11–15] were generally numerical because of the large number of propagating fields and the fact that the interaction between the fields is nonlinear. Only in a special circumstance,[1] such as the consideration of both a single Stokes shift and zero pump retroreflection, can the model for the Raman fiber laser yield an analytical solution for the output. In addition, because of the large number of Stokes fields generated in recent demonstrations of cascaded Raman fiber lasers, especially those relying on either germano-doped or pure silica for the Raman gain, numerical computation of the pump and intracavity Stokes fields becomes compulsory. Some recent investigations of the numerical simulation of Raman fiber lasers[13,15] deal with the issues relating to specific fibers and to particular experiments. However, in this investigation, we examine the general characteristics of Raman fiber lasers by studying the Stokes cavity modes as the order of the Raman fiber laser is changed. The output dependence on the fiber length, output mirror reflectivity, and cavity losses is also examined, as is customary with most numerical simulations of Raman fiber lasers. However, we also study the time dependence of the Stokes cavity modes as the pump power to the Raman fiber laser is modulated.

Unlike most reports on the numerical simulation of the Raman fiber laser,[11–15] we also present for completeness a detailed explanation of the numerical methods used to calculate the characteristics of the Raman fiber laser. The well-known system of BVODEs, mentioned above, has the standard form usually assumed in the literature, e.g., Ref. 16. Each boundary condition is separated, in that it is applied at either endpoint of the problem interval, but not both. For such systems there has been a considerable amount of research on the development of numerical algorithms and, over the past three decades, a number of high-quality, robust, and efficient packages have been developed. These include the PASVAR3 code,[17]

which employs finite-difference methods within a deferred correction framework, the COLSYS and COLNEW packages,[18,19] which employ collocation methods, the TWPBVP package,[20] which employs Runge–Kutta methods within a deferred correction algorithm, and the MIRKDC code,[21] which uses Runge–Kutta methods within a defect-control algorithm. All these codes employ adaptive mesh selection algorithms to handle difficult solution behavior and use sophisticated modified Newton methods to solve efficiently the nonlinear algebraic systems that arise. They generally employ structured Gaussian elimination software to efficiently solve linear systems, and global-error estimation and control (or, in the case of MIRKDC, defect estimation and control) to ensure that a reliable solution is obtained.

In much of the literature on the study of the problem of numerical simulation of cascaded Raman fiber lasers, little is said about the numerical approach, and in fact, many authors seem to have developed their own numerical techniques. We note an exception to this in Ref. 15, in which the COLSYS code, mentioned above, is employed. In fact, any of the BVODE codes mentioned in the preceding paragraph would be a reasonable choice for the treatment of the problem. In our investigation we employ the MIRKDC package. We have written software modules that describe the corresponding differential equations and boundary conditions for an arbitrary nth-order Raman fiber laser; this software calls MIRKDC to solve the resultant system. We provide further details concerning the numerical algorithms employed by MIRKDC in a later section. We have found that the MIRKDC package was able to solve a wide variety of model problems, characterized by various n values, as well as by values for the many other parameters describing the problem. Our choice of MIRKDC is motivated by our need to examine a time-dependent extension of the original BVODE system. The extension to time-dependent problems requires substantial modification to the underlying BVODE code, and we chose MIRKDC because we are familiar with the implementation details and the source code; hence the extensive modifications required to the code were quite straightforward.

Although our primary interest is the investigation of the steady-state system that is described by BVODEs, we have also included in this paper some discussion of a preliminary treatment of a corresponding time-dependent version of this family of problems. The time dependence is introduced by assuming that the initial pump power exhibits a periodic time-dependent modulation. The usual ordinary differential equations (ODEs) are therefore augmented with time derivatives. The resulting system of partial differential equations (PDEs) bears a strong relationship in structure to the standard ODE system; it is thus natural to consider a numerical treatment of the PDE system with an approach known as the transverse method of lines, see, e.g., Ref. 16. In this approach the time derivatives are replaced with finite differences and the result is a larger system of BVODEs that contains one copy of the original system of BVODEs for each time step of the discretized time variable. It is then possible, with only minor modifications to the original software modules, to treat this larger BVODE system with the MIRKDC package. Although the difficulty of this new system of BVODEs does not increase (MIRKDC is still able to solve the problem using only a very coarse mesh), the substantially larger number of BVODEs means that the execution time for each run of the program increases dramatically. However, by performing a modification to the MIRKDC code to allow for careful treatment of the linear-algebra computations, it is possible to attain significant improvements in performance.

2. THEORY

An nth-order cascaded Raman fiber laser (see Fig. 1) is composed of a silica-based fiber a few hundred meters in length and Bragg gratings placed at each end in order to resonate the intracavity Stokes fields. In most numerical treatments of cw cascaded Raman fiber lasers,[11–13] consideration of both the forward- and the backward-traveling fields is not carried out and only the local intensity is calculated. In accordance with the notation used in Ref. 14 (we introduce first the full PDE system describing a cascaded Raman fiber laser), the classical treatment of the stimulated Raman scattering processes resulting in nth-order Stokes output from a cascaded Raman fiber laser in the slowly varying field approximation is given by the following equations:

$$\begin{aligned}\frac{1}{P_0^+(z,t)}\left[\frac{\partial P_0^+(z,t)}{\partial z}+\frac{n}{c}\frac{\partial P_0^+(z,t)}{\partial t}\right]&=\frac{1}{-P_0^-(z,t)}\left[\frac{\partial P_0^-(z,t)}{\partial z}+\frac{n}{c}\frac{\partial P_0^-(z,t)}{\partial t}\right]\\&=-\alpha_0-\frac{\omega_0}{\omega_1}\gamma_1[P_1^+(z,t)+P_1^-(z,t)],\end{aligned}\tag{1}$$

$$\begin{aligned}\frac{1}{P_i^+(z,t)}\left[\frac{\partial P_i^+(z,t)}{\partial z}+\frac{n}{c}\frac{\partial P_0^+(z,t)}{\partial t}\right]&=\frac{1}{-P_i^-(z,t)}\left[\frac{\partial P_i^-(z,t)}{\partial z}+\frac{n}{c}\frac{\partial P_i^-(z,t)}{\partial t}\right]\\&=-\alpha_i+\gamma_i[P_{i-1}^+(z,t)+P_{i-1}^-(z,t)]\\&\quad-\gamma_{i+1}\frac{\omega_i}{\omega_{i+1}}[P_{i+1}^+(z,t)+P_{i+1}^-(z,t)]\\&\quad\text{for } i=1 \text{ to } n-1,\end{aligned}\tag{2}$$

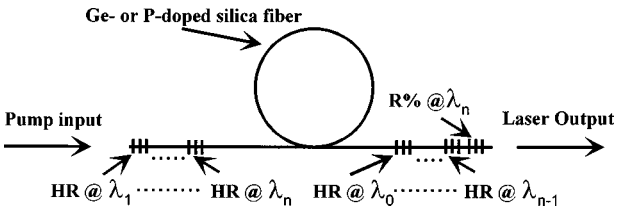

Fig. 1. Schematic diagram of an nth-order cascaded Raman fiber laser. HR represents a highly reflecting Bragg grating, and R% indicates a Bragg grating with <100% reflectivity at the nth Stokes wavelength. λ_n represents the wavelength of the nth Stokes cavity mode.

$$\frac{1}{P_n^+(z,t)}\left[\frac{\partial P_n^+(z,t)}{\partial z}+\frac{n}{c}\frac{\partial P_n^+(z,t)}{\partial t}\right]$$
$$=\frac{1}{-P_n^-(z,t)}\left[\frac{\partial P_n^-(z,t)}{\partial z}+\frac{n}{c}\frac{\partial P_n^-(z,t)}{\partial t}\right]$$
$$=-\alpha_n+\gamma_n[P_{n-1}^+(z,t)+P_{n-1}^-(z,t)]. \quad (3)$$

The positive and negative superscripts in Eqs. (1)–(3) represent the forward- and backward-propagating pump (P_0) and Stokes (P_i, in W) fields, respectively. Spontaneous Raman scattering has been neglected because it is assumed that Raman oscillation is dominant, and it is assumed that all of the fields are unpolarized and that axial symmetry exists. The coefficients α_i, are the values of the intrinsic loss of the host glass at the various field wavelengths, and ω_0 and ω_i are the frequencies of the pump and ith Stokes fields, respectively. The experimentally determined Raman-gain coefficient γ_i for unpolarized light is given by $\gamma_i = 4.89 \times 10^{-14}/(\lambda/A_{\text{eff}})$, where λ_i is the wavelength (in micrometers) of the ith Stokes wave and A_{eff} is the effective core area.[14] In this study we used the actual core area and not the area relevant to each optical mode. The assumption of a pure-silica gain coefficient in the model means that these simulations relate to systems that have the P_2O_5 or GeO_2 content (necessary for the required wavelength shift) fixed at a level that provides approximately the same γ_i as for pure silica.

The boundary conditions for an nth-order cascaded Raman fiber laser at the input end to the fiber are given by

$$P_0^+(0) = P_{\text{Launch}} + R_0 P_0^-(0), \quad (4a)$$

$$P_i^+(0) = P_i^-(0) \quad \text{for } i = 1 \text{ to } n. \quad (4b)$$

At the output end to the fiber, the boundary conditions are given by

$$P_i^-(L) = P_i^+(L) \quad \text{for } i = 0 \text{ to } (n-1), \quad (5a)$$

$$P_n^-(L) = R_n P_n^+(L). \quad (5b)$$

R_0 is the reflectivity of the pump light at the input end to the fiber, and R_n is the reflectivity of the nth Stokes mode at the output end of the fiber. P_{Launch} is the launched pump power, and it is assumed that the high reflectivities of the various fields are ideally 100%. For the time-dependent case, initial conditions for all x are required; we assume that the initial solution for the time-dependent problem is the solution yielded by the corresponding steady-state case.

Under steady-state conditions the pump and the Stokes photons obey, in the absence of loss and with equal Raman gain for all wavelengths, the following conservation of momentum relation:

$$\frac{\mathrm{d}}{\mathrm{d}z}\left[\sum_{i=1}^{n}\frac{\omega_0}{\omega_i}P_i^+(z)+P_0^+(z)\right]$$
$$-\frac{\mathrm{d}}{\mathrm{d}z}\left[\sum_{i=1}^{n}\frac{\omega_0}{\omega_i}P_i^-(z)+P_0^-(z)\right]=0. \quad (6)$$

For the first part of the investigation we will be concerned with the steady-state operation of a cascaded Raman fiber laser. The equations describing this problem can be easily obtained from Eqs. (1)–(3) by neglecting the time dependence ($\partial/\partial t = 0$) and setting all partial derivatives to normal derivatives.

It has been shown[12,13] that taking into account the overlap of the various intracavity fields with the core of the fiber is important in determining realistic conversion efficiencies. In the present investigation we have neglected this aspect to elucidate the general trends and the overall issues concerning the Raman fiber laser system.

3. NUMERICAL METHOD

A. MIRKDC and the Treatment of Steady-State Problems

The software used to solve the systems of first-order nonlinear BVODEs (the MIRKDC package, available in the 'netlib'[22] numerical software collection) is based on discrete and continuous mono-implicit Runge–Kutta methods, e.g., Ref. 23 and the references therein. The code provides continuous solution and derivative approximations across the entire problem interval. Monitoring the defect of the computed solution controls the solution quality. The approximate solution computed by MIRKDC is required to have a defect that is less than a user-provided tolerance.

The computation is based on a mesh that subdivides the problem interval. Through the course of the computation the mesh is modified by the MIRKDC code to allow it to adapt to regions of difficult solution behavior. The Runge–Kutta methods are used to discretize the ODEs, leading to a set of nonlinear algebraic equations. These are solved by a Newton iteration; various forms of Newton iteration to improve the performance damped Newton iterations with adaptive selection of damping factors and fixed Newton matrix iterations are employed. The Newton matrices have a special sparsity structure known as almost-block diagonal.[24] This structure has a block-bidiagonal form; there are two blocks associated with each subinterval, and the dimension of each block is equal to the number of ODEs. These Newton systems are efficiently treated with the COLROW software package.[25,26] The dominant computational costs are in the setup and the solution of these almost-block-diagonal linear systems. These costs are linear in the number of subintervals but, since matrix multiples are involved in the setup of each block and a special form of Gaussian elimination is used to solve the almost-block-diagonal system, these costs are cubic in the dimension of the blocks, i.e., cubic in the number of ODEs. More details are available in Refs. 21 and 27.

For many of the problems we considered (by selecting specific choices for all the parameters), we found that MIRKDC was able to obtain a solution in a reasonably straightforward fashion, using quite small meshes of only about ten subintervals and with only a few Newton iterations. For some problems the crude initial-solution approximation we provided (either straight lines through the boundary conditions or zero) was not sufficient to obtain convergence of the Newton iteration. In these cases we employed the standard device of parameter continua-

tion; that is, we solved a sequence of progressively more difficult problems, using the final mesh and solution from one problem as the initial mesh and solution for the next. We found that this additional technique allowed us to solve all of the desired steady-state problems.

Since the steady-state problems in this study involve at most 12 ODEs and the number of mesh subintervals was small, the computational time was very short; all individual problems and even the problems treated in parameter-continuation sequences could be solved in only a few seconds.

B. Treatment of Time-Dependent Problems by the Transverse Method of Lines

The general approach in this part of the investigation was to attempt to treat the time-dependent case with as little modification as possible to the software. This led to the use of the transverse method of lines. In this approach the system of partial differential equations is transformed into a (larger) system of BVODEs by discretizing in time. This means that a partition of the time dimension is selected, e.g., division of the time dimension into 100 equal time steps. We then associate a new solution variable, dependent only on the spatial dimension, with each time step. That is, if the solution to the system of partial differential equations is $u(t, x)$ and the ith time-step value is t_i, then we define $y_i(x) = u(t_i, x)$. The time derivatives are then replaced with first-order backward differences, and with some rearrangement of terms, one obtains a large system of BVODEs in x, in terms of the unknowns, $y_i(x)$.

A significant point here is that the number of BVODEs obtained from this approach is the number of partial differential equations times the number of time steps. Thus for the Stokes order-5 case the number of PDEs is 12, and if we use 100 time steps, the resultant BVODE system will consist of 1200 equations. In Subsection 3.A we mentioned that the primary computational costs of the MIRKDC code were associated with the linear-algebra computations and that these are cubic in the number of equations. Although a system of 12 BVODEs (the steady-state Stokes problem with Stokes order 5) can be solved in <0.02 s, we can see that the time-dependent case, involving 1200 equations, should take $\sim 10^6$ times as long. We observed this in practice; the MIRKDC code took ~ 8 h to solve one of the time-dependent problems. However, by paying careful attention to the linear-algebra computations, we were able to achieve substantial savings in the computation time. Although the Jacobian matrices associated with the large BVODE system were matrices of dimension 1200 by 1200, they were very sparse. By carefully adapting to these sparsity structures, it was possible to drastically reduce the costs of the matrix multiplications by a factor of approximately 100. The second major modification involved replacing the direct linear-system solver COLROW with iterative sparse linear-system software. This led to further massive decreases in the overall computation time. The resultant modified MIRKDC code was able to solve the time-dependent problem that involved the system of 1200 BVODEs in ~ 4 min.

4. RESULTS

We generated calculations from the model using the experimental conditions related to a relatively recent demonstration of a >1-W 1.48-μm cascaded Raman fiber laser.[5] With this particular system, the second P_2O_5 Raman peak (at 1396 cm^{-1}) was used twice from a start wavelength of 1.06 μm. We also confine our simulations to the generation of ~ 1.48-μm radiation because most cascaded Raman fiber laser demonstrations to date produce this output wavelength because of the implications this wavelength has in the telecommunications industry.

The calculated intracavity fields from the model as a function of distance along the fiber are shown in Fig. 2. One observes that the pump [Fig. 2(a)] is gradually converted to first Stokes radiation as it propagates along the fiber with the point at which the pump power decreases to e^{-1} of its launched value located 495 m from the input end to the fiber. The values of the forward- and reverse-propagating Stokes fields [Fig. 2(b)] are clamped (at the same value) at each end of the fiber as a result of the boundary conditions imposed on the Stokes field, and this, combined with the gradual decay of the pump beam, forces the maximum in the Stokes field to locate approximately in the center of the fiber. The consequence of these effects is to shape the first Stokes cavity mode into a fundamental standing-wave pattern with the antinode approximately in the center of the fiber and the nodes at each end. We also observe that pump retroreflection has a beneficial effect on the overall efficiency of the present fiber laser arrangement. The significantly higher output power of 2.02 W calculated from the model as compared

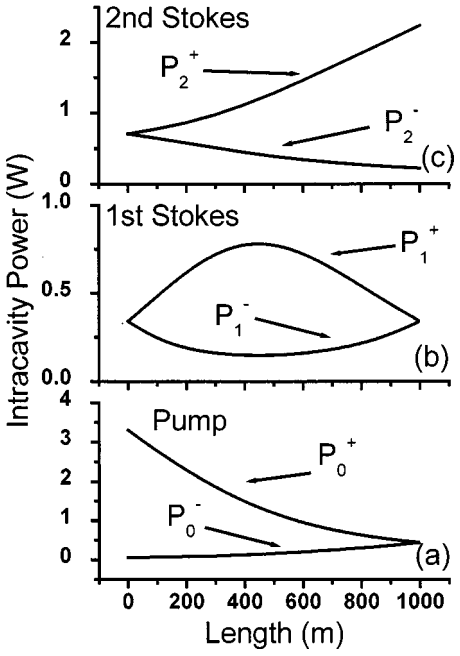

Fig. 2. Calculated values of (a) the pump, (b) the first Stokes, and (c) the second Stokes cavity modes as a function of length along the second-order cascaded Raman fiber laser. For this simulation the launched pump power was 3.3 W, fiber length was 1000 m, core diameter was 5 μm, and the reflectivity of the second Stokes radiation at the output end of the fiber was 10%. Potential excess losses as a result of splices, etc., were neglected, $\alpha_0 = 1.7$ dB/km, and $\alpha_1 = \alpha_2 = 1$ dB/km.

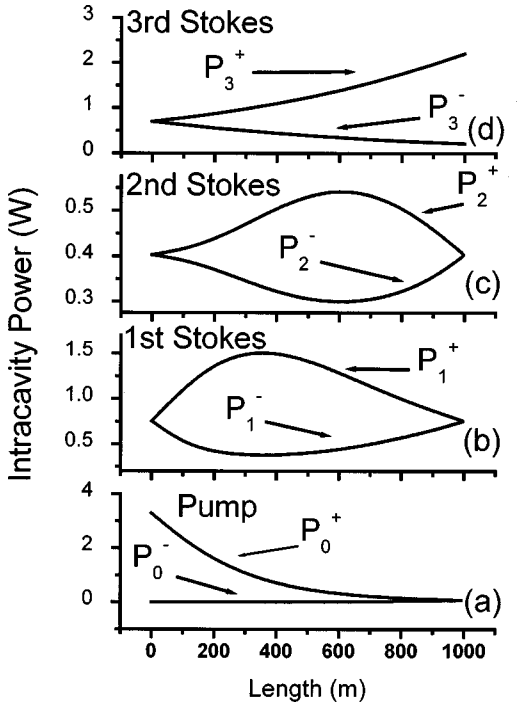

Fig. 3. Calculated values of (a) the pump, (b) the first Stokes, (c) the second Stokes, and (d) the third Stokes cavity modes as a function of length along the third-order cascaded Raman fiber laser. For this simulation the launched pump power was 3.3 W, fiber length was 1000 m, core diameter was 5 μm, the reflectivity of the third Stokes radiation at the output end of the fiber was 10%. Potential excess losses as a result of splices, etc., were neglected, $\alpha_0 = 1.7$ dB/km, and $\alpha_1 = \alpha_2 = \alpha_3 = 1$ dB/km.

with the measured value of 1.1 W[5] primarily relates to the fact that, in this simulation, we use a larger value of the output coupling (90% cf. 85%) and we neglect excess losses arising from splices, mode mismatch, etc.

An alternative method of generating 1.48-μm radiation would involve a third-order cascaded Raman process, i.e., one could use the second P_2O_5 Raman peak to generate 1.24 μm, and the first P_2O_5 Raman peak (at 648 cm^{-1}) twice to generate Stokes wavelengths at 1.348 and 1.477 μm and supplying the second and third Stokes fields, respectively. Therefore, this system becomes a practical fiber-laser simulation in which to compare with the above results. The results of the third-order calculation related to the above configuration are presented in Fig. 3. We observe that the calculated pump [Fig. 3(a)] is depleted comparatively more quickly as a result of the larger first Stokes cavity mode now present (the point at which the pump power decreases to e^{-1} of its start value is now located 273 m from the input end to the fiber). The calculated first and second Stokes cavity modes are both fundamental standing waves for reasons already outlined above; however, the first Stokes cavity mode has its antinode located closer to the input end of the fiber. This is a result of the combination of the smaller second Stokes cavity mode in this region of the fiber (which produces a lower loss term in the equation for first Stokes fields) and the larger pump intensity in this region (producing a larger gain term). The combined effect of these two processes is to shift the peak in this cavity mode toward the input end of the fiber. The calculated value of the output power from this laser is calculated to be only ~2% lower at 1.98 W as compared with the above second-order system.

The calculations from the model for a fourth-order cascaded Raman fiber laser designed to provide 1.46-μm radiation is presented in Fig. 4. For a practical demonstration of this system, four Stokes shifts on the first P_2O_5 Raman peak at 648 cm^{-1} would make available four Stokes fields with wavelengths of 1.138, 1.229, 1.335, and 1.46 μm. We note first that the calculated second Stokes cavity mode [Fig. 4(c)] is a standing wave of a higher order, with a node 330 m from the input end to the fiber. If we examine the forward-propagating field of the calculated second Stokes cavity mode, we observe that the antinode is located 165 m from the input end to the fiber because of the relatively large first Stokes cavity mode and the lower third Stokes cavity mode [Fig. 4(d)] in this region; the opposite is true for the reverse propagating second Stokes cavity mode, which has an antinode (1000 − 330)/2 = 670 m from the input end to the fiber. The pump power decays similarly to the pump decay relevant to the second-order cascaded Raman fiber laser with the point at which the pump power decreases to e^{-1} of its start value located 440 m from the input end to the fiber. The calculated output power from this simulation is calculated to be 1.66 W, some 18% lower as compared with the second-order calculation.

The calculations from the model for a fifth-order cascaded Raman fiber laser also providing 1.46-μm radiation

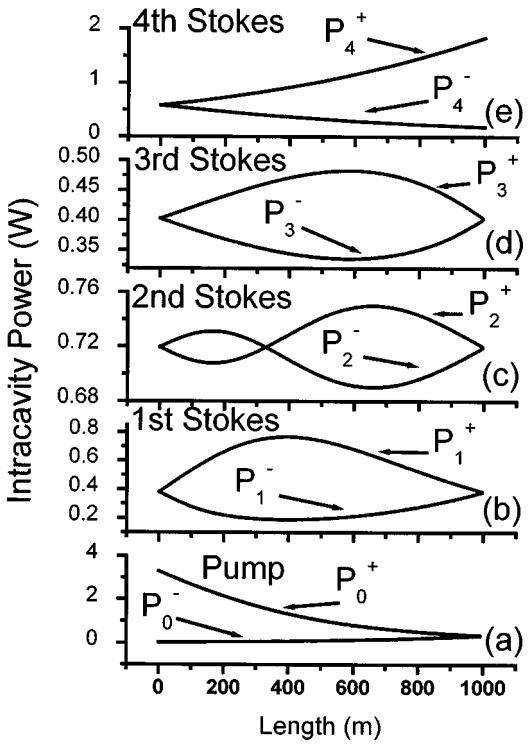

Fig. 4. Calculated values of (a) the pump, (b) the first Stokes, (c) the second Stokes, (d) the third Stokes, and (e) the fourth Stokes cavity modes as a function of length along the fourth-order cascaded Raman fiber laser. For this simulation the launched pump power was 3.3 W, fiber length was 1000 m, and the reflectivity of the fourth Stokes radiation at the output end of the fiber was 10%. Potential excess losses arising from splices, etc., were neglected, $\alpha_0 = 1.7$ dB/km, and $\alpha_1 = \alpha_2 = \alpha_3 = \alpha_4 = 1$ dB/km.

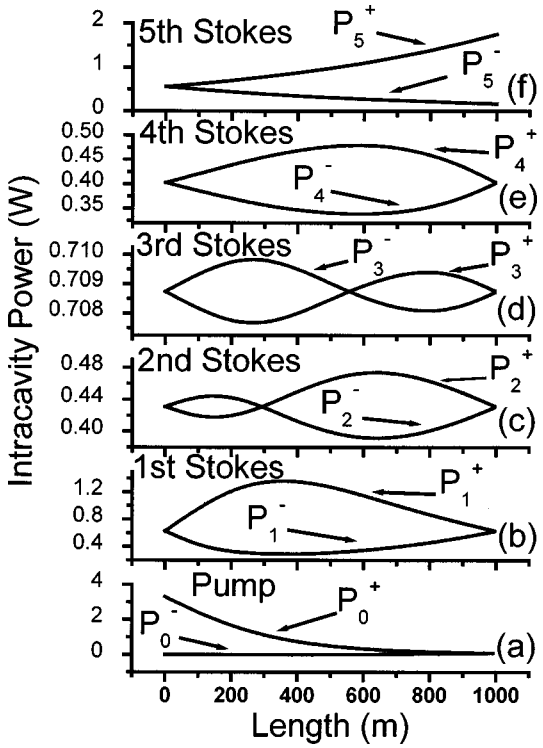

Fig. 5. Calculated values of (a) the pump, (b) the first Stokes, (c) the second Stokes, (d) the third Stokes, (e) the fourth Stokes, and (f) the fifth Stokes cavity modes as a function of length along the fifth-order cascaded Raman fiber laser. For this simulation the launched pump power was 3.3 W, fiber length was 1000 m, core diameter was 5 μm, and the reflectivity of the fifth Stokes radiation at the output end of the fiber was 10%. Potential excess losses arising from splices, etc., were neglected, $\alpha_0 = 1.7$ dB/km, and $\alpha_1 = \alpha_2 = \alpha_3 = \alpha_4 = \alpha_5 = 1$ dB/km.

is presented in Fig. 5. Likewise, for a practical demonstration of this system, five Stokes shifts starting on the main SiO_2 Raman peak at 440 cm^{-1} and alternating between this SiO_2 Raman peak and the first P_2O_5 Raman peak at 648 cm^{-1} would provide the required Stokes fields at wavelengths of 1.112, 1.198, 1.26, 1.372, and 1.46 μm. We note first that the calculated second and third Stokes cavity modes [Figs. 5(c) and 5(d)] are higher-order standing waves. The second Stokes cavity mode has a node that is 290 m and the third Stokes cavity mode has a node that is 555 m from the input end to the fiber. The Stokes cavity modes adjacent to the pump and the output Stokes cavity modes are, as in the above examples, of the fundamental type; see Figs. 5(b) and 5(e). The pump power decays similarly to the pump power relevant to the third-order cascaded Raman fiber laser with the point at which the pump power decreases to e^{-1} of its start value located 282 m from the input end to the fiber. The calculated output power from this simulation is calculated to be 1.58 W, some 22% lower as compared with the second-order calculation.

The calculated slope efficiency of the output for the second-order cascaded Raman fiber laser as a function the length of the fiber and the amount of excess loss (i.e., losses arising from splices, etc.) is shown in Fig. 6(a). We observe, as with other numerical studies of the cascaded Raman fiber laser,[13,15] that the slope efficiency varies almost linearly with the change in the length of the fiber. This is obvious since the parameter that influences the slope efficiency in this case is the overall intrinsic loss of the glass, a parameter that gradually increases proportionally as the length of the fiber is increased. For zero excess loss the slope efficiency decreases by ~2% per 100 m and decreases to ~1.3% per 100 m when the excess loss is 1 dB because, as the excess losses become dominant, the effect on the slope efficiency as a result of the length-dependent intrinsic losses becomes smaller. We calculated that for zero intrinsic loss the maximum slope efficiency is ~66%, which is very close to the Stokes-efficiency limit of ~72%.

The calculated pump power at threshold as a function of fiber length and excess loss for a second-order fiber laser is presented in Fig. 6(b). As expected, an increase in the excess loss produces an increase in the threshold pump power, especially for short fiber lengths, because it is the dominant loss mechanism. As the fiber length is increased, however, the pump power at threshold decreases, as was observed in other numerical studies.[12,13,15] This decrease in the pump power at threshold reflects the gradual increase in the length-integrated Raman gain; however, as the length of the fiber is increased beyond the point that has the length-integrated gain greater than the loss, the pump power at

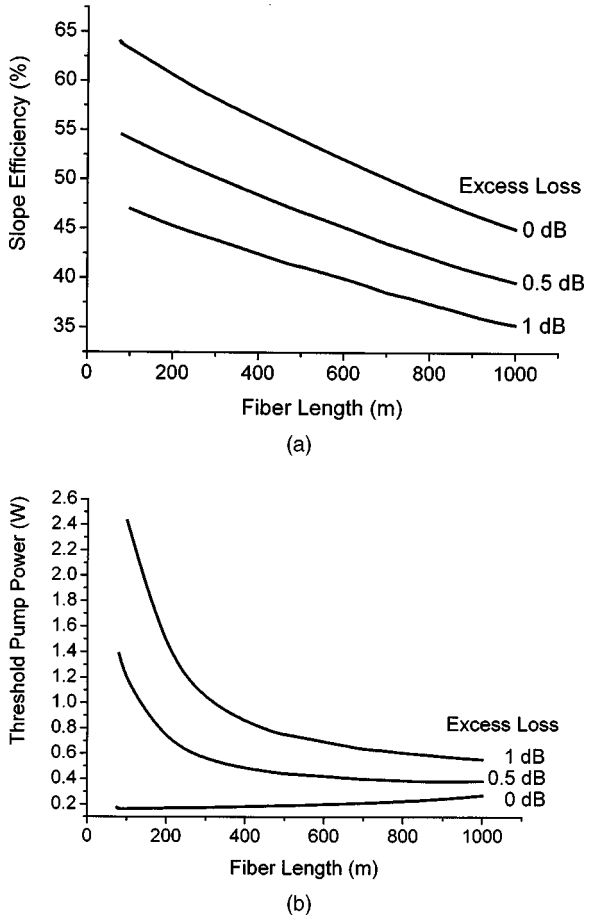

Fig. 6. Calculated values of (a) the slope efficiency and (b) the pump power at threshold for a second-order cascaded Raman fiber laser. For this simulation the reflectivity of the second Stokes radiation at the output end of the fiber was 15%, core diameter was 5 μm, $\alpha_0 = 1.7$ dB/km, and $\alpha_1 = \alpha_2 = 1$ dB/km.

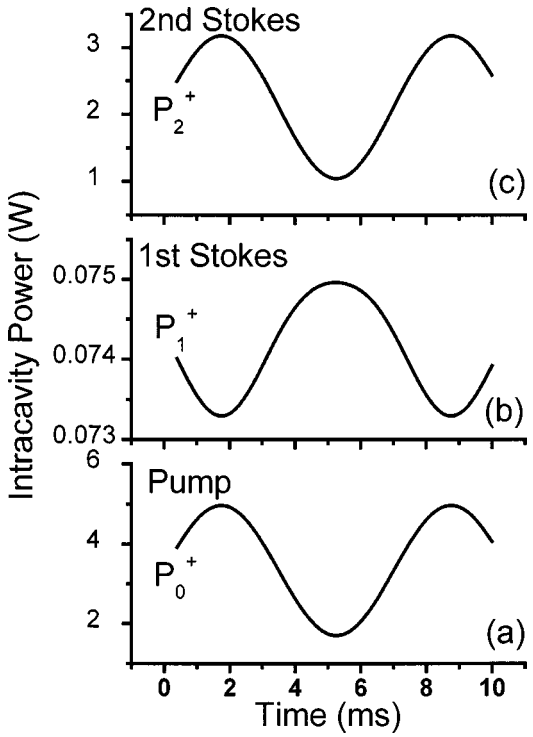

Fig. 7. Calculated values of (a) the pump (taken at $z = 0$), (b) the forward-propagating first Stokes cavity mode (taken at $z = 1000$ m), and (c) the forward-propagating second Stokes cavity mode (taken at $z = 1000$ m) as a function of time for sinusoidal modulation of the pump. The pump modulation had a 50% modulation depth, a 7 ms period, and 3.3-W time-averaged launched power. The fiber length was 1000 m, core diameter was 5 μm, and the second Stokes reflection coefficient was 95% (i.e., 5% output coupling).

threshold will increase. For the cascaded Raman fiber laser example discussed here, this will occur when the fiber length is >1000 m. To establish a correct length of fiber for optimized performance, one could define a figure of merit as the ratio of the slope efficiency to the pump power at threshold, as in previous studies.[11,13] Using this, we find that the optimized length increases as the excess loss increases; however, for excess losses <0.5 dB, fiber lengths in the 200–400-m range will provide optimized performance.

For the results of the time-dependent case, a problem in which we varied the pump with a sinusoidal modulation, we ensured that the modulation period was significantly longer than the round-trip time of the cavity. Round-trip effects such as spontaneous emission can be ignored, and the stimulated-emission and absorption processes are still the dominant mechanisms of the Raman fiber laser. In the results presented below, we used a modulation period of 7 ms throughout, considered a fiber length of 1000 m, and confined our investigation to a second-order cascaded Raman fiber laser. Considering that it takes photons 10 μs for a round trip for a fiber of this length, a modulation period of 7 ms represents approximately 700 round trips, and consequently, to a first approximation, Eqs. (1)–(3) are valid.

Modulating the pump to a depth of 50% [Fig. 7(a)], and while maintaining an average launched pump power of 3.3 W, we observe that the calculated first Stokes cavity mode [Fig. 7(b)] oscillates with a similar modulation characteristic, but with a $\pi/2$ phase difference. Such behavior is typical of antiphase dynamics. We observe that for the 50% pump modulation the calculated first Stokes cavity mode oscillates with only a ~1% modulation depth, significantly smaller than that of the pump. The modulation of the second Stokes cavity mode [Fig. 7(c)], however, oscillates in phase with the pump but with a modulation depth of 52%. When the second Stokes reflection coefficient was reduced to 10%, the modulation depth of the calculated first Stokes cavity mode increased to ~19%, and the modulation depth of the calculated second Stokes cavity mode increased to ~54%. From these calculations we can infer that there exists a direct correlation between the modulation depths of the various Stokes fields and the Q of the cavity of the nth Stokes order.

Increasing the modulation depth of the pump to 100% [Fig. 8(a)], the calculated temporal characteristics of the Stokes cavity modes become significantly altered. Figure 8(b) displays the resultant first Stokes cavity mode oscillation. The out-of-phase first Stokes modulation is now split into two separate subpulses that are spaced 1.68 ms apart and have pulse widths of ~0.33 ms. The in-phase second Stokes cavity mode [Fig. 9(c)] is zero within the region $t = 4.41$ ms to $t = 6.09$ ms; the region in which the first Stokes cavity mode oscillates. The first Stokes pulse splits because the pump power falls below the Raman fi-

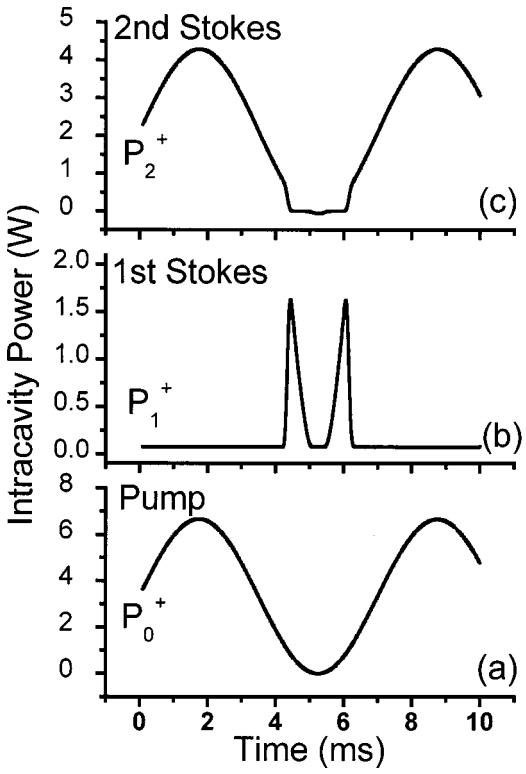

Fig. 8. Calculated values of (a) the pump (taken at $z = 0$), (b) the forward-propagating first Stokes cavity mode (taken at $z = 1000$ m), and (c) the forward-propagating second Stokes cavity mode (taken at $z = 1000$ m) as a function of time for sinusoidal modulation of the pump. The pump modulation had a 100% modulation depth, a 7 ms period, and 3.3-W time-averaged launched power. The fiber length was 1000 m, the core diameter was 5 μm, and the second Stokes reflection coefficient was 95% (i.e., 5% output coupling).

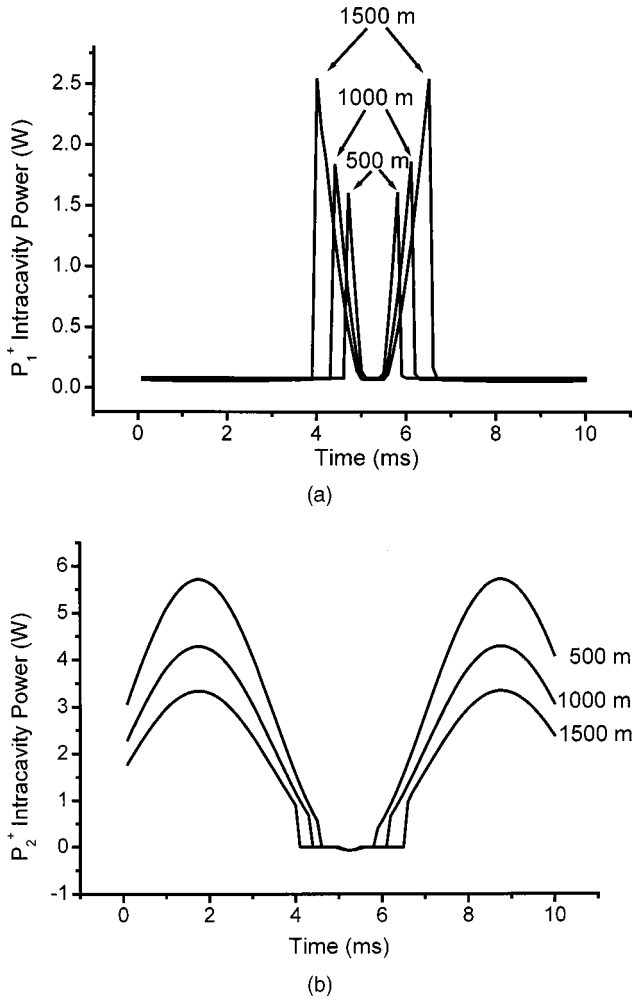

Fig. 9. Calculated values of (a) the forward-propagating first Stokes cavity mode (taken at $z = L$), and (b) the forward-propagating second Stokes cavity mode (taken at $z = L$) for sinusoidal modulation of the pump as a function of time and for various values of the fiber length. The pump modulation had a 100% modulation depth, a 7-ms period, and 3.3-W time-averaged launched power. The second Stokes reflection coefficient was 95% (i.e., 5% output coupling), and the core diameter was 5 μm.

ber laser threshold value during this part of the modulation. Changing the length of the fiber changes the calculated pulse separation and pulse widths of the subpulses relevant to the first Stokes cavity mode modulation, as can be observed in Fig. 9(a). For a fiber length of 1500 m, the calculated subpulse separation widens to 2.43 ms and the pulsewidth lengthens to ~0.41 ms, as compared with the fiber of 1000-m length. For a fiber length of 500 m, however, the subpulse separation is narrowed to 1.1 ms and the pulse width shortens to ~0.21 ms. The period of time in which the second Stokes cavity mode oscillation is zero becomes gradually wider as the length of the fiber is increased [see Fig. 9(b)].

5. DISCUSSION

Numerically modeling the propagation of the forward and reverse Stokes fields has given insight into the behavior of the Stokes modes as the order of the cascaded Raman fiber laser is changed. When the output wavelength was kept approximately the same for all of the cascaded Raman fiber lasers examined, a direct comparison between the characteristics of the cascaded Raman fiber lasers was enabled.

The numerical treatment of the steady-state problems was accomplished by employing a standard software package for systems of nonlinear BVODEs. When coupled with a simple parameter-continuation algorithm, the MIRKDC code was able to solve all the steady-state problems we considered in a straightforward fashion. The spatial meshes employed were quite coarse, and little adaptive mesh selection was required. The numerical treatment of the time-dependent problems was accomplished by a simple modification of the software developed for the steady-state case, based on the transverse method of lines. The time dependence arising in the systems of PDEs was treated with a simple finite-difference scheme, leading to a large system of BVODEs, which could then be solved with the MIRKDC code. Owing to the large number of BVODEs, several special modifications to the linear-algebra computations within MIRKDC were implemented to obtain significant improvements in the computation time. One such improvement involved replacing the block linear-system solver with a sparse, banded solver. An interesting area for future research would be to compare this approach with a treatment of the PDEs using a conventional method-of-lines algorithm.

An additional parameter affecting the performance of cw cascaded Raman fiber lasers is the reflectivity of the output coupler of the final Stokes cavity mode. Increasing (to 90%) the reflection coefficient of the output coupler relevant to the second Stokes cavity mode of the second-order cascaded Raman fiber laser presented in Fig. 2 will increase the value of the intracavity power of this mode. This will have the affect of increasing the loss term relevant to the first Stokes cavity mode, and therefore the value of the intracavity power of first Stokes mode will be considerably lower compared with the power shown in Fig. 2(b). Further, as a result of this power decrease, the decay (conversion) rate of the pump will be reduced (the point at which the pump power decreases to e^{-1} of its start value is now located 1400 m from the input end to the fiber). In addition, 0.78 W of the 3.3-W launched pump power is actually transmitted through the pumped end of the fiber. For the third-order cascaded Raman fiber laser, also with a 90%-reflectivity output coupler, the relatively large value of the intracavity third Stokes mode power forces a lower value of the second Stokes mode power, which, in turn, allows a relatively large first Stokes mode power to resonate. This obviously forces a rapid decay of the pump (e^{-1} of its start value located 100 m from the input end) and although no apparent waste of the pump occurs, the energy is locked up in maintaining relatively large resonant Stokes cavity modes. Overall, the amplitudes of the Stokes cavity modes adjust so as to maintain a relative balance between the loss and the gain of each Stokes mode and generally results in alternating high and low values for the power of each mode. As for most laser systems, choice of the appropriate output coupler for a given level of pump power is paramount to maximizing the efficiency of the system.

As far as the time-dependent problem is concerned, when the reflectivity of the output coupler of the nth Stokes cavity was large, the value of the $(n-1)$th Stokes field was correspondingly smaller. Only a small modulation of the $(n-1)$th Stokes field was therefore required for a large modulation of the nth Stokes field since the nth Stokes was produced from a relatively small $(n-1)$th field. When the reflectivity of the nth Stokes field was decreased to 10%, the value of the nth Stokes field was correspondingly smaller, implying a larger $(n-1)$th Stokes field. This latter field required a stronger modulation depth to significantly modulate the nth Stokes field.

One of the important parameters highlighted in recent numerical investigations of cascaded Raman fiber lasers[11,13,15] is the length of the fiber for Raman gain. In general, a fiber that is too short will not provide enough length-integrated gain to overcome the losses of the system, and hence the threshold will not be reached. In contrast, a fiber that is too long will introduce excessive loss as a result of the increased intrinsic losses of the fiber, and the overall efficiency will be low. Of the recent demonstrations of cascaded Raman fiber lasers, most experiments have involved fibers that are $\geqslant\sim$1000 m;[5–8] however, one relatively early example[3] and some quite recent demonstrations[28,29] have involved the use of fiber lengths that are less than 500 m. From the above results it is clear those fiber lengths in the range 100–500 m will most likely result in more optimal performance from the cascaded Raman fiber laser.

The antiphase dynamics observed when the pump is modulated result from the coupling that occurs between the Stokes cavity modes because of the cross-saturation terms P_iP_{i+1} in Eqs. (1)–(3). Since the coupling occurs between only the nearest neighbors, a cascaded Raman fiber laser could be considered as consisting of a chain of locally coupled nonlinear oscillators, similar to the longitudinal modes of a highly multimode Nd^{3+}-doped silica fiber laser that has the characteristics of having the inhomogeneous broadening significantly wider than the homogeneous broadening.[30,31] In the case of a Nd^{3+}-doped silica fiber laser the homogeneous broadening provides the range in which coupling takes place, and the inhomogeneous broadening provides the total length of the oscillator chain. It is conceivable, for a sufficiently high-order cascaded Raman fiber laser (the total number of oscillators comprising the chain is $n+1$), that perturbing one of the Stokes cavity modes, i.e., by modifying its intensity, for example, the phase and group velocities of the perturbation will have opposite signs as the perturbation moves along the chain of oscillators. Further investigations into the temporal behavior of cascaded Raman fiber lasers are currently taking place.

6. CONCLUSION

We have studied in detail the performance of nth-order cascaded Raman fiber lasers using the partial differential equations relating to stimulated-emission and intrinsic-absorption processes only. We have established that the forward- and reverse-propagating Stokes fields together form standing-wave cavity modes. The patterns are generally of a fundamental type when they are adjacent to either the pump or the nth Stokes cavity mode. Intermediate Stokes cavity modes, however, oscillate with a higher-order standing wave, depending on the value of n. Preliminary calculations relating to the time-dependent problem, which has the pump modulated sinusoidally, reveal that the Stokes cavity modes oscillate with antiphase dynamics typical of a system of locally coupled nonlinear oscillators. For a second-order cascaded Raman fiber laser we observe pulse splitting of the calculated second Stokes cavity mode when the modulation depth of the pump is increased to 100%.

For our investigation of the steady-state problems we have developed software for describing the BVODE systems associated with cascaded Raman fiber lasers for a given Stokes order, which when coupled with the MIRKDC package, was able to solve all the problems we investigated in a straightforward fashion. The treatment of a time-dependent version of this problem was undertaken with a numerical approach known as the transverse method of lines; this involved only minor modifications to the software describing the steady case, but to obtain substantial improvements in execution time, extensive changes to the linear-algebra components of MIRKDC, to employ sparse matrix multiplications and a sparse, iterative, linear-system solver, were required. These modifications to the MIRKDC code led to massive improvements in execution time, and we were then able to solve all the time-dependent problems considered in this investigation.

ACKNOWLEDGMENTS

The authors thank the Australian Photonics Cooperative Research Centre and the Natural Sciences and Engineering Research Council of Canada for financial support.

REFERENCES

1. J. AuYeung and A. Yariv, "Theory of cw Raman oscillation in optical fibers," J. Opt. Soc. Am. **69**, 803–807 (1979).
2. P. Persephonis, S. V. Chernikov, and J. R. Taylor, "Cascaded CW Raman laser source 1.6-1.9 μm," Electron. Lett. **32**, 1486–1487 (1996).
3. E. M. Dianov, M. V. Grekov, I. A. Bufetov, S. A. Vasiliev, O. I. Medvedkov, V. G. Plotnichenko, V. V. Koltashev, A. V. Belov, M. M. Bubnov, S. L. Semjonov, and A. M. Prokhorov, "CW high power 1.24 μm and 1.48 μm Raman lasers based on low loss phosphosilicate fibre," Electron. Lett. **33**, 1542–1544 (1997).
4. S. V. Chernikov, N. S. Platonov, D. V. Gapontsev, D. I. Chang, M. J. Guy, and J. R. Taylor, "Raman fibre laser operating at 1.24 μm," Electron. Lett. **34**, 680–681 (1998).
5. V. I. Karpov, E. M. Dianov, V. M. Paramonov, O. I. Medvedkov, M. M. Bubnov, S. L. Semyonov, S. A. Vasiliev, V. N. Protopopov, O. N. Egorova, V. F. Hopin, A. N. Guryanov, M. P. Bachynski, and W. R. L. Clements, "Laser-diode-pumped phosphosilicate-fiber Raman laser with an output power of 1 W at 1.48 μm," Opt. Lett. **24**, 887–889 (1999).
6. E. M. Dianov, I. A. Bufetov, M. M. Bubnov, M. V. Grekov, A. V. Shubin, S. A. Vasil'ev, O. I. Medvedkov, S. L. Semenov, O. N. Egorova, A. N. Gur'yanov, V. F. Khopin, M. V. Yashkov, D. Dvarelas, A. Iocco, D. Costantini, H. G. Limberger, and R.-P. Salathe, "Continuous-wave highly efficient phosphosilicate fibre-based Raman laser (λ=1.24 μm)," Kvant. Elektron. (Moscow) **29**, 97–100 (1999).
7. N. S. Kim, M. Prabhu, C. Li, J. Song, and K. Ueda, "1239/1484 nm cascaded phosphosilicate Raman fiber laser with

CW output power of 1.36 W at 1484 nm pumped by CW Yb-doped double-clad fibre laser at 1064 nm and spectral continuum generation," Opt. Commun. **176**, 219–222 (2000).
8. E. M. Dianov, I. A. Bufetov, M. M. Bubnov, M. V. Grekov, S. A. Vasilev, and O. I. Medvedkov, "Three-cascaded 1407-nm Raman laser based on phosphorous-doped silica fiber," Opt. Lett. **25**, 402–404 (2000).
9. S. G. Grubb, T. Strasser, W. Y. Cheung, W. A. Reed, V. Mizrahi, T. Erdogan, P. J. Lemaire, A. M. Vengsarkar, and D. J. DiGiovanni, "High power, 1.48 μm cascaded Raman laser in germanosilicate fibers," in *Optical Amplifiers and Their Applications*, Vol. 18 of OSA Technical Digest Series (Optical Society of America, Washington, D.C., 1995), pp. 197–199.
10. S. A. E. Lewis, S. V. Chernikov, and J. R. Taylor, "1.4 W saturated output power from a fiber Raman amplifier," in *Optical Fiber Communication Conference*, 1999, OSA Technical Digest Series (Optical Society of America, Washington, D.C., 1999), pp. 114–116.
11. W. A. Reed, W. C. Coughran, and S. G. Grubb, "Numerical modelling of cascaded cw Raman fiber amplifiers and lasers," in *Optical Fiber Communication Conference*, Vol. 8 of OSA Technical Digest Series (Optical Society of America, Washington, D.C., 1995), pp. 107–108.
12. A. Bertoni, "Analysis of the efficiency of a third order cascaded Raman operating at the wavelength of 1.24 μm," Opt. Quantum Electron. **29**, 1047–1058 (1997).
13. A. Bertoni and G. C. Reali, "1.24-μm cascaded Raman laser for 1.31-μm Raman fiber amplifiers," Appl. Phys. B **67**, 5–10 (1998).
14. G. Vareille, O. Audouin, and E. Desurive, "Numerical optimisation of power conversion efficiency in 1480 nm multi-Stokes Raman fibre lasers," Electron. Lett. **34**, 675–676 (1998).
15. M. Rini, I. Cristiani, and V. Degiorgio, "Numerical modeling and optimization of cascaded CW Raman fiber lasers," IEEE J. Quantum Electron. **36**, 1117–1122 (2000).
16. U. M. Ascher, R. M. M. Mattheij, and R. D. Russell, *Numerical Solution of Boundary Value Problems for Ordinary Differential Equations*, Classics in Applied Mathematics Series (SIAM, Philadelphia, 1995).
17. M. Lentini and V. Pereyra, "An adaptive finite difference solver for nonlinear two-point boundary problems with mild boundary layers," SIAM J. Numer. Anal. **14**, 94–111 (1977).
18. U. M. Ascher, J. Christiansen, and R. D. Russell, "Collocation software for boundary value ODE's," ACM Trans. Math. Software **7**, 209–222 (1981).
19. G. Bader and U. M. Ascher, "A new basis implementation for a mixed order boundary value ODE solver," SIAM J. Sci. Stat. Comput. **8**, 483–500 (1987).
20. J. R. Cash and M. H. Wright, "A deferred correction method for nonlinear two-point boundary value problems: implementation and numerical evaluation," SIAM J. Sci. Stat. Comput. **12**, 971–989 (1991).
21. W. H. Enright and P. H. Muir, "Runge–Kutta software with defect control for boundary value ODE's," SIAM J. Sci. Stat. Comput. **17**, 479–497 (1996).
22. www.netlib.org.
23. P. H. Muir, "Optimal discrete and continuous mono-implicit Runge–Kutta schemes for BVODE's," Adv. Comput. Math. **10**, 135–167 (1999).
24. P. Amodio, J. R. Cash, G. Roussos, R. W. Wright, G. Fairweather, I. Gladwell, G. L. Kraut, and M. Paprzycki, "Almost block diagonal linear systems: sequential and parallel solution techniques, and applications," Numer. Linear Algebra Appl. **7**, 275–317 (2000).
25. J. C. Diaz, G. Fairweather, and P. Keast, "Algorithm 603. COLROW and ARCECO: FORTRAN packages for solving certain almost block diagonal linear systems by modified alternate row and column elimination," ACM Trans. Math. Software **9**, 376–380 (1983).
26. J. C. Diaz, G. Fairweather, and P. Keast, "FORTRAN packages for solving certain almost block diagonal linear systems by modified alternate row and column elimination," ACM Trans. Math. Software **9**, 358–375 (1983).
27. W. H. Enright and P. H. Muir, "A Runge–Kutta type boundary value ODE solver with defect control," Dept. Comput. Sci. Tech. Rep. 93-267 (University of Toronto, Toronto, Ontario, Canada, 1993) (http://www.cs.toronto.edu/NA/reports.html#cs-93-267).
28. M. Prabhu, N. S. Kim, L. Jianren, and K. Ueda, "Simultaneous two-color CW Raman fiber laser with maximum output power of 1.05 W/1239 nm and 0.95 W/1484 nm using phosphosilicate fiber," Opt. Commun. **182**, 305–309 (2000).
29. D. I. Chang, M. Y. Jeon, H. K. Lee, and K. H. Kim, "1480~1485 nm cascaded CW Raman fiber laser," in *Conference on Lasers and Electro-Optics*, Vol. 39 of OSA Trends in Optics and Photonics (Optical Society of America, Washington, D.C., 2000), pp. 302.
30. C. Szwaj, S. Bielawski, and D. Derozier, "Propagation of waves in the spectrum of a multimode laser," Phys. Rev. Lett. **77**, 4540–4543 (1996).
31. C. Szwaj, S. Bielawski, and D. Derozier, "Acoustical and optical branches in the spectral waves of a laser," Phys. Rev. A **57**, 3022–3027 (1998).